(Received 22 January 2026, Accepted 24 February 2026, Scheduled 2 April 2026)

Compact Elliptical Multi-Band Microstrip Sensor for Thumb-Tissue Glucose Sensing

Amjad H. Yousif[1], Saad W. O. Luhaib[1,*], and Mohammed Y. Thanoun[2]

[1] *Department of Electrical Engineering, College of Engineering, University of Mosul, Mosul, Iraq*
[2] *Department of Communications and Intelligent Digital Systems Engineering, College of Engineering University of Mosul, Mosul, Iraq*

ABSTRACT: This paper presents a new compact triple-band elliptical microstrip resonator for noninvasive microwave-based glucose sensing using a thumb-contact configuration. The proposed sensor employs concentric elliptical rings with a localized slot and capacitive coupling to enhance electric-field confinement in the sensing region. A multilayer cylindrical thumb phantom incorporating dispersive tissue models and glucose-dependent blood permittivity is utilized to emulate realistic on-body conditions. Full-wave simulations in the 2–6 GHz band demonstrate three dominant glucose-sensitive resonances with monotonic frequency shifts over a concentration range of 0–600 mg/dL. The frequency deviation rates are 0.147, 0.64, and 1.037 MHz/(mg/dL), respectively, with the highest linearity reaching $R^2 \approx 0.98$. By distributing sensing across multiple resonant modes, the proposed approach enables frequency-diverse feature extraction suitable for multivariate regression, improving robustness against contact variability and tissue heterogeneity compared to single-band configurations.

1. INTRODUCTION

Diabetes mellitus (DM) is a chronic metabolic disorder characterized by persistent hyperglycaemia and impaired insulin secretion and/or action, leading to long-term complications that affect cardiovascular, renal, neural, and visual systems [1]. The global burden of diabetes continues to increase, imposing substantial health and economic impacts worldwide [2]. Conventional self-monitoring of blood glucose (SMBG) relies on finger-prick capillary measurements, which can be painful and inconvenient, and these barriers may reduce adherence to routine daily use [3, 4].

Continuous glucose monitoring (CGM) systems provide near real-time interstitial glucose trends and alarms, improving glycemic management compared to intermittent SMBG in many settings [3, 5]. However, CGM remains minimally invasive (subcutaneous sensor) and may entail cost and wearability limitations, and user experience varies across populations, motivating the continued development of fully noninvasive alternatives [6].

Among noninvasive sensing modalities, microwave techniques have attracted growing attention because glucose-related changes in tissue dielectric properties can modulate the near-field response of resonant structures [7, 8]. Planar microstrip resonators are particularly appealing owing to their compactness, low fabrication cost, and strong electric field confinement, which support high spectral selectivity for sensing applications [7, 9].

Despite this promise, reliable on-body glucose estimation remains challenging owing to confounding factors, such as inter-subject variability, hydration, temperature, motion, and weak perturbations associated with physiological glucose changes [9, 10]. Recent studies have explored multi-frequency or multi-band microwave sensors to increase information content and improve robustness. For example, dual-band resonant sensors have been demonstrated in both *in-vitro* and on-body configurations [11, 12]. A dual-band resonator combined with machine learning has been reported for noninvasive monitoring using a human-subject protocol [13, 14].

A broad variety of resonant configurations have been investigated, including microstrip and split-ring resonators, complementary split-ring resonators (CSRRs), patch resonators, Goubau lines, and plasmonic microwave structures. These designs have been evaluated both in vitro using aqueous or tissue-mimicking phantoms and in on-body scenarios [5–10].

Recent contributions include a high-figure-of-merit surface plasmonic microwave resonator wrapped around the human arm, demonstrating glucose-correlated variations in frequency and amplitude near 3.25 and 4.67 GHz [7]. A dual-band band-pass filter sensor operating at 2.45 and 5.2 GHz has also been proposed, where machine-learning models were integrated to enhance prediction accuracy [8]. In addition, a multi-band monopole antenna incorporating split-ring resonators has been developed for continuous noninvasive monitoring across multiple resonances between 0.94 and 6.3 GHz [9]. Furthermore, complementary split-ring resonator (CSRR)-based and triple-pole structures have been investigated to exploit multiple resonant modes within the centimetre wave range and improve sensitivity [10].

* Corresponding author: Saad Wasmi Osman Luhaib (s.w.o.luhaib@uomosul.edu.iq).

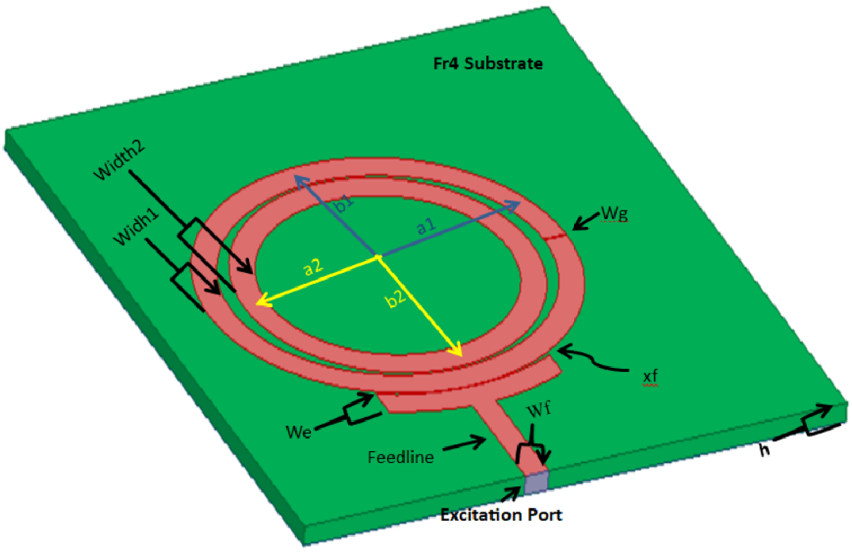

FIGURE 1. Triple bands elliptical ring resonator sensor for non-invasive glucose.

These studies collectively indicate that multi-band and metamaterial-inspired resonators can improve sensitivity and provide redundant frequency-domain features suitable for robust regression or machine-learning frameworks. Given that most commercial SMBG devices sample blood from fingertips, the finger and thumb represent particularly attractive anatomical sites for microwave-based sensing; for instance, investigations on thumb placement over elliptical resonators have quantified the influence of positioning on sensitivity and repeatability [11]. Related studies have demonstrated that variability in fingertip fat-pad thickness significantly modifies the scattering parameters of CSRR-based sensors, thereby affecting permittivity estimation and glucose prediction [12].

Nonetheless, many existing finger- and thumb-oriented microwave sensors still operate at only one or two resonances, span a limited glucose range (often up to $\approx$ 200 mg/dL), or rely mainly on simplified phantom models without systematically exploiting multiple resonant bands in a single compact device [5, 7, 10–12]. Therefore, key challenges persist in achieving high frequency sensitivity with quasi-linear responses over the full physiologically relevant range (from hypoglycemia to severe hyperglycemia), ensuring robustness to thumb positioning and tissue thickness variations, and extracting multiple independent features from a practical, thumb-mounted platform that can be integrated into low-cost measurement systems [5, 6, 13].

In this work, a compact triple-band elliptical microstrip resonator is proposed. The design enables the simultaneous extraction of multiple frequency features, improving sensitivity, linearity, and robustness under realistic thumb-loading conditions.

2. PROPOSED TRI-BANDS DIABETES SENSOR AND MODELING

The proposed sensor consists of a concentric triple-band elliptical ring microstrip resonator etched on the top surface of an FR-4 substrate ($\epsilon_r = 4.4$, $\tan\delta = 0.02$) backed by a continuous ground plane, as illustrated in Fig. 1.

The sensing structure is formed by two closely spaced elliptical copper rings with a narrow azimuthal gap in the outer ring that defines the open-ended resonator and concentrates the electric field in a localized sector beneath the future thumb or phantom placement region. A 50 Ω microstrip feed line is aligned tangentially to the rings and terminated in a small coupling gap to the outer ring, enabling electric-field coupling while preserving a compact footprint suitable for integration in portable platforms. The inner ring is dimensioned and positioned to introduce additional resonant paths and modal interactions, thereby generating multiple resonant frequencies within the targeted microwave band and enhancing the sensitivity to permittivity perturbations in the near-field region above the rings. To obtain the initial dimensions of the proposed elliptical ring resonator, the target resonance frequencies are calculated using the well-known resonance relation for a microstrip ring resonator [15]:

$$f_r = \frac{n\,c}{2\pi\, r_{mean}\sqrt{\varepsilon_{eff}}} \tag{1}$$

where n is the mode index, c the speed of light in free space, and ϵ_{eff} the effective dielectric constant of the microstrip structure. By rearranging, the expression for the mean radius can be rewritten to provide the practical design rules.

$$r_{mean} = \frac{n\,c}{2\pi f\sqrt{\varepsilon_{eff}}} \tag{2}$$

Because the proposed resonator employs elliptical rather than circular rings, each ring is characterized by a major semi-axis a and minor semi-axis b. An equivalent mean radius is defined by equating the area of the ellipse to that of a circle with radius r_{mean}, which is simplified to

$$r_{mean}^2 \approx a_{mean}\, b_{mean} \tag{3}$$

To control the ellipticity of the resonator, a constant aspect ratio is introduced as

$$k = \frac{a_{mean}}{b_{mean}} \tag{4}$$

Combining the above relations yields closed-form expressions for the average semi-axes in terms of the equivalent mean radius:

$$\begin{aligned} b_{mean} &= \frac{r_{mean}}{\sqrt{k}} \\ a_{mean} &= r_{mean}\sqrt{k} \end{aligned} \tag{5}$$

The actual outer and inner elliptical rings are then obtained by adding and subtracting half of the strip width wth_i:

$$\begin{aligned} a_{1,i} &= a_{mean,i} + \frac{wth_i}{2} \\ a_{2,i} &= a_{mean,i} - \frac{wth_i}{2} \end{aligned} \tag{6}$$

$$\begin{aligned} b_{1,i} &= b_{mean,i} + \frac{wth_i}{2} \\ b_{2,i} &= b_{mean,i} - \frac{wth_i}{2} \end{aligned} \tag{7}$$

Thus, $(a_{1,i}, b_{1,i})$ represents the outer (far) contour of each elliptical ring, and $(a_{2,i}, b_{2,i})$ represents the inner (near) contour.

The closed-form expressions above are used only to provide an initial sizing of the triple-band elliptical rings. In practice, these dimensions are subsequently refined through a systematic parametric sweep and optimization procedure in the High Frequency Structure Simulator (HFSS). Table 1 summarizes the geometric parameters used to describe the configuration of the concentric dual-ring microstrip resonator.

TABLE 1. Dimensions of the proposed triple-band elliptical sensor configuration.

Dimensions	Symbol	Value (mm)
Substrate width	W_s	70
Substrate length	L_s	70
Substrate thickness	h_s	1.6
Outer ellipse major semi-axis	a_1	20.7
Outer ellipse minor semi-axis	b_1	17.7
Outer ellipse strip width	Wth_1	3
Inner ellipse major semi-axis	a_2	18
Inner ellipse minor semi-axis	b_2	20
Inner ellipse strip width	Wth_2	2
Feed line width	W_f	3
Feed line extension width	W_e	3
Gap (feed to outer ellipse)	X_f	0.15
Thump center position (x, y)	(c_x, c_y)	(0, 19.8)
Slot width in outer ellipse	W_g	0.15

The geometric parameters were fine-tuned using the HFSS optimization module around their nominal values to accurately

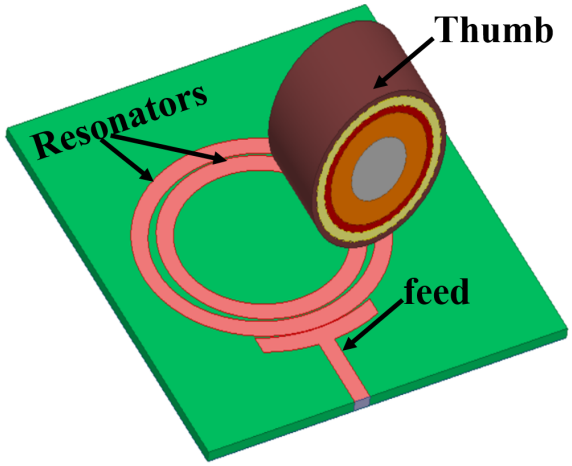

FIGURE 2. Position of thumb on sensor.

position the desired resonant frequencies. The presence of the thumb or glucose-equivalent sample above the outer ring at $(c_x, c_y) = (0, 19.8)$, as shown in Fig. 2, ensured that the sample was positioned directly over the high-$|E|$ sector, while the inter-ring coupling path remained spatially separated from the loading region. This arrangement reduces the direct perturbation of the coupling mechanism by the thumb and improves the stability and consistency of the sensor response. Moreover, the elliptical geometry provides an additional advantage by allowing the coupling region to be distributed away from the thumb location, while keeping the loading effectively concentrated on the outer ring. As a result, the resonance frequency shift exhibited a more monotonic and linear trend with glucose variation, leading to improved linearity within the investigated concentration range.

To account for the interaction between the sensor and thumb, a multilayer equivalent model of the finger pulp consisting of skin, fat, muscle, blood, and bone layers stacked above a thin air window (0.1 mm) covering the sensor aperture was used. Each finger tissue is modeled using a frequency dispersive Debye/Cole-Cole expression, while the blood layer is made explicitly dependent on the glucose concentration. To emulate the thumb loading conditions, a cylindrical, multilayer phantom was positioned directly above the high-electric-field region of the resonator. The phantom comprises concentric cylindrical shells, representing the skin, subcutaneous fat, muscle, cortical bone, and central blood region. Each layer is assumed homogeneous and isotropic, with a complex relative permittivity $\varepsilon_r^*(f)$ described by Debye/Cole–Cole-type models fitted to canonical dielectric data available in the literature and the IT'IS Foundation tissue database [14–17].

In the Cole-Cole framework, the complex relative permittivity of a generic tissue layer can be written as

$$\varepsilon_r^*(\omega) = \varepsilon_\infty + \sum_{n=1}^{N} \frac{\Delta\varepsilon_n}{1 + (j\omega\tau_n)^{1-\alpha_n}} + \frac{\sigma}{j\omega\varepsilon_0}, \tag{8}$$

where ε_∞ denotes the effective high-frequency permittivity; $\Delta\varepsilon_n$ and τ_n represent, respectively, the strength and characteristic relaxation time of the n-th dispersion region; α_n accounts

for the distributed nature of relaxation times in biological media (with $\alpha_n = 0$ reducing to an ideal Debye relaxation); and σ is the ionic conductivity contributing to the imaginary part of ε_r^* through the term $\sigma/(j\omega\varepsilon_0)$.

A single-pole Debye form with glucose-dependent parameters was adopted for glucose-dependent blood (or blood-equivalent solution) [14]:

$$\varepsilon^*_{blood}(\omega, C_x) = \varepsilon_\infty(C_x) + \frac{\Delta\varepsilon_1(C_x)}{1 + j\omega\tau_1} + \frac{\sigma_{dc}(C_x)}{j\omega\varepsilon_0}, \quad (9)$$

where $\omega = 2\pi f$, ε_0 is the permittivity of free space, $\tau_1 = 1.5 \times 10^{-11}$ s, and C_x is the glucose concentration in mg/dL. Glucose dependence is introduced via second-order polynomials in C_x:

$$\varepsilon_\infty(C_x) = 0.0099C_x^2 + 0.047C_x + 2.3, \quad (10)$$

$$\Delta\varepsilon_1(C_x) = -0.0093C_x^2 - 0.21C_x + 71, \quad (11)$$

$$\sigma_{dc}(C_x) = 0.0063C_x^2 - 0.14C_x + 2, \quad (12)$$

obtained by curve fitting to the reported complex-permittivity data for glucose-water/blood-plasma solutions in the microwave band [14, 19].

The surrounding thumb tissues are modeled using glucose-independent Debye-type expressions with fixed parameters of bone, fat, muscle, and skin:

$$\varepsilon^*_{bone}(\omega) = 11.4 + \frac{0.39}{j\omega\varepsilon_0}, \quad (13)$$

$$\varepsilon^*_{fat}(\omega) = 5.28 + \frac{0.1}{j\omega\varepsilon_0}, \quad (14)$$

$$\varepsilon^*_{muscle}(\omega) = 54.8 + \frac{2.26}{j\omega\varepsilon_0}, \quad (15)$$

$$\varepsilon^*_{skin}(\omega) = 4 + \frac{39}{1 + j\omega\tau_2} + \frac{1.46}{j\omega\varepsilon_0}, \quad (16)$$

with $\tau_2 = 7.96 \times 10^{-12}$ s. These parameters are consistent with the parametric models in [14, 16] and tabulated tissue properties in [17].

This combined sensor-thumb model allows the accurate prediction of the three resonance frequencies and their $|S_{11}|$ minima as functions of the blood glucose concentration, forming the basis for the regression and sensitivity analysis presented in the following sections.

Figure 3 illustrates the multilayer thumb phantom employed to emulate realistic thumb loading over the high electric field region of the sensor. The phantom was modeled as a finite-length cylinder composed of concentric cylindrical shells, where the layers represent (from the center outward) bone, muscle, blood, fat, and skin. The geometric specifications of the cross-section are summarized in Table 2 in terms of the outer in-plane dimensions of each concentric shell together with the corresponding layer thickness, ensuring a consistent and anatomically plausible stratified structure within the simulation window. Table 2 lists the electromagnetic parameters assigned to each tissue layer (relative permittivity and loss tangent). They collectively governed the dielectric loading and attenuation imposed on the resonator during thumb placement. This multilayer representation offers a physically interpretable approximation of the thumb pulp anatomy and allows for a systematic evaluation of how glucose-induced perturbations affect it.

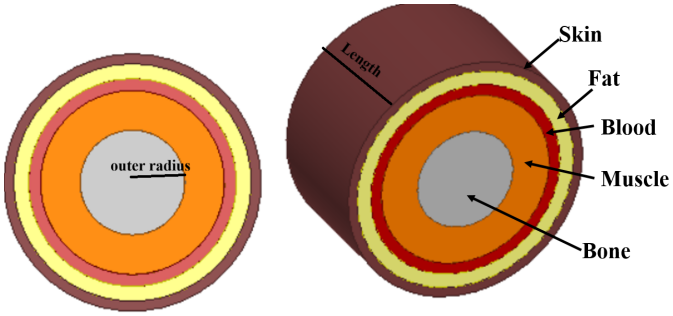

FIGURE 3. Thumb phantom layers.

TABLE 2. Thumb phantom dimensions and electromagnetic properties.

Layer	Length × Outer radius (mm)	Thickness (mm)	ε_r	tanδ
Bone	14 × 4.3	4.3	11.4	0.25
Muscle	14 × 6.8	2.5	54.8	0.24
Blood	14 × 7.8	1.0	59.0	0.31
Fat	14 × 9.0	1.2	5.3	0.16
Skin	14 × 10.0	1.2	43.0	0.30

3. RESULTS AND DISCUSSION

Figure 4 presents the simulated reflection coefficient $|S_{11}|$ of the thumb-loaded sensor at $C_x = 0$ mg/dL. Three dominant resonant modes are observed at approximately 2.054 GHz, 2.83 GHz, and 5.128 GHz. These resonances constitute the reference baseline for evaluating glucose-induced frequency shifts under loaded conditions.

Figure 5 shows the reflection-coefficient ($|S_{11}|$) response of the thumb-loaded sensor for glucose concentrations $c = 0$, 100, and 200 mg/dL, with five resonance bands, where $|S_{11}|$ falls below -3 dB located approximately at 2.1–2.2 GHz, 2.7–2.9 GHz, 3.3–3.6 GHz, 4.7–4.9 GHz, and 5.1–5.5 GHz. A com-

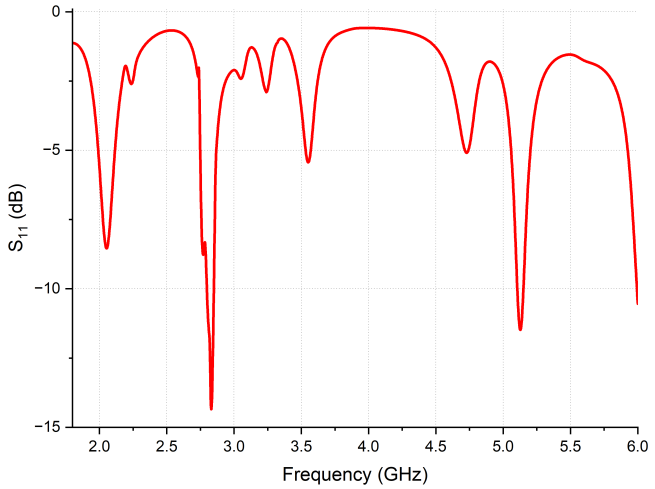

FIGURE 4. Simulated $|S_{11}|$ response of the thumb-loaded sensor at $C_x = 0$ mg/dL.

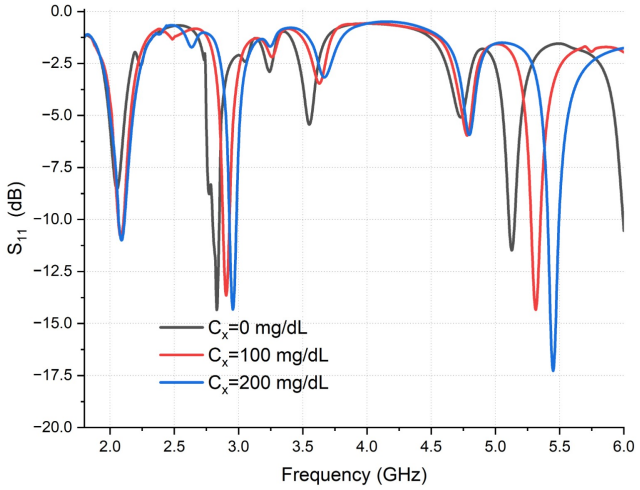

FIGURE 5. The simulation response of the sensor under different glucose concentrations.

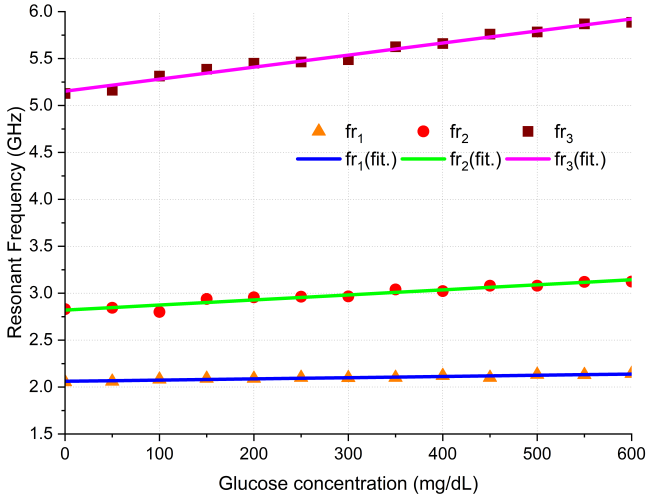

FIGURE 6. Real and fitting resonant frequencies versus glucose concentration.

parison of the three curves across these bands indicated that the corresponding resonance frequencies experienced only modest shifts as c increased. In particular, in the bands near 2.8 GHz and 3.4 GHz, the changes in resonant frequency are small and irregular (nonlinear with respect to concentration), indicating negligible frequency sensitivity to glucose in these regions. Similarly, in the middle bands around 3.4 and 4.7 GHz, the positions of the minima move by only a few hundred of megahertz, while even in the highest band near 5.1 GHz, where the response is most pronounced, the resonances for different concentrations remain confined within a narrow frequency interval.

Figure 6 presents the variation in the three most significant resonant bands as a function of glucose concentration (C_x) in the extended range 0–600 mg/dL, showing a clear, nearly linear increase in resonant frequency with (C_x) in all cases. Band 1 shifts from approximately 2.1 GHz at 0 mg/dL to about 2.2 GHz at 600 mg/dL, whereas band 2 moves from roughly 2.7 GHz to around 3.2 GHz over the same interval. The highest band (band 3) exhibits the largest absolute change, with its resonance increasing from about 5.1 GHz to beyond 5.8 GHz as the concentration rises. The monotonic and almost linear behaviour observed in Fig. 6 confirms that these three bands are the most glucose-sensitive modes of the sensor and are therefore well-suited for inclusion in regression or machine-learning models aimed at estimating blood-glucose concentration from measured frequency shifts. The key metric is the frequency-detection resolution (FDR), expressed in MHz/(mg/dL), which can be obtained from the frequency-concentration sensors as in [17]

$$\mathrm{FDR}_i = \frac{\Delta f_i}{\Delta C_x} \tag{17}$$

where Δf_i is the frequency shift in each band, and ΔC_x is the variation in glucose. Normalized sensitivity, reported in 1/(mg/dL), was used as the basis for fair sensor comparison [18].

$$S_i = \frac{\mathrm{FDR}_i}{f_{i0}} \times 100 \tag{18}$$

where f_{i0} is the frequency value at 0 mg/dL glucose consecration for bands 1 and 2.

3.1. Frequency Sensitivity and Linearity Metrics

Table 3 illustrates a compact quantitative summary for each band. f_1 and f_2 represent the resonance frequency at 0 mg/dL and 600 mg/dL, respectively, while $f_{0,avg}$ represents the average resonance frequency over the considered range.

Band 2 clearly provides the largest absolute and normalized sensitivity, with FDR =0.64 MHz/(mg/dL) and $S \approx 0.012\%$/(mg/dL). Band 3 exhibited a slightly lower FDR, but still a strong response, whereas band 1 was the least sensitive. In terms of linearity, band 3 achieved an excellent coefficient of determination ($R^2 \approx 0.98$), indicating an almost ideal linear relationship between frequency and glucose concentration. Band 2 maintains good linearity ($R^2 \approx 0.90$) but with more pronounced local fluctuations, whereas band 1 shows the lowest R^2 (≈ 0.82), reflecting its higher sensitivity to noise and small modelling uncertainties.

Physically, the higher sensitivity of band 2 is consistent with the stronger dispersive behavior of the lossy biological medium around its resonant frequency, where both dielectric relaxation and conductive losses contribute significantly to the complex permittivity. The superior linearity of band 3 suggests that, in this frequency region, the effective permittivity of the thumb phantom varies with glucose in a more monotonic and quasi-linear manner, making band 3 particularly attractive for simple calibration models. Band 1, although less sensitive and less linear, provides a useful low-frequency observable that can be exploited as an additional feature in multi-band regression.

3.2. Comparison with Literature and Multi-Band Perspective

The normalized sensitivities obtained here, on the order of 10^{-3}–10^{-2}%/(mg/dL), are comparable to those reported for planar resonant microwave glucose sensors using aqueous or blood-equivalent samples. In many published single-band designs, a single dominant resonance is tuned to maximize fre-

TABLE 3. Summary of sensitivity and linearity metrics for the triple bands.

Band	f_1 @ 0 mg/dL (GHz)	f_2 @ 600 mg/dL (GHz)	$f_{0,\text{avg}}$ (GHz)	FDR (MHz/mg/dL)	S (%/mg/dL)	R^2
Band 1	2.054	2.142	2.098	0.147	0.7	0.0.819
Band 2	2.83	3.214	3.022	0.64	0.021	0.923
Band 3	5.128	5.75	5.439	1.037	0.019	0.9794

TABLE 4. Comparison of microwave-based glucose sensing techniques.

Ref.	**Concentration (mg/dL)**	**Frequency (GHz)**	**Sensitivity (MHz/(mg/dL))**	**Size (mm^2)**	**MUT**
[7]	89–262	5.5, 8.5	3.53, 3.58	450	Fingertip
[8]	89–456	2.32	0.95	–	Aqueous glucose
[9]	0–400	2.45, 5.2	0.9	40 × 40	Aqueous glucose/finger
[14]	–	1.7	0.089	–	Thumb
[15]	0–500	4.5, 9.2	0.6	20 × 30	Aqueous glucose
[16]	60–150	1.5	1.099	20 × 66	Dual finger
[17]	0–16000	4.187	0.00187	60 × 60	Aqueous glucose
[18]	–	5.77	1.87	40 × 40	On-body monitoring
[19]	60–200	14	0.571	15 × 15	Semi-solid tissue-mimicking phantom
[20]	50–250	3.1	0.75	60 × 20	Aqueous glucose (glass container to mimic fingertip)
This work	0–600	2.054, 2.83, 5.128	0.147, 0.64, 1.037	70 × 70	Thumb phantom

quency excursion over a relatively narrow glucose interval. In contrast, the present sensor deliberately distributes the sensing function over three coupled modes within the 2–6 GHz band.

This multi-band strategy has several advantages. First, it provides redundant information under the same thumb-loading condition, which improves the robustness of the estimation with respect to noise, contact variability, and inter-subject differences. Second, it enables the use of multivariate regression or machine learning frameworks, where the triple-band (fr_1, fr_2, fr_3) serves as a frequency-diverse feature vector that enhances selectivity and reduces the impact of confounding tissue parameters compared with single-frequency measurements. Third, it allows internal consistency checks, for example, by monitoring whether the three bands follow the expected joint trend, which can act as built-in quality indicators for each measurement.

Within this framework, the proposed tri-band sensor can be interpreted as a multi-channel resonant probe. Band 1 offers moderate sensitivity but is relatively tolerant to loading perturbations; band 2 acts as the primary high-sensitivity channel; and band 3 combines very high linearity with a sensitivity comparable to that of band 1, making it particularly valuable for stabilising multi-band regression models. A natural next step, addressed in a separate section of this work, is to fit the glucose concentration as a function of the three resonances:

$$C_{\text{est}} = \beta_0 + \beta_1 fr_1 + \beta_2 fr_2 + \beta_3 fr_3, \tag{19}$$

and to quantify the improvement in R^2 and the prediction error with respect to the single-band model $C_{\text{est}}(f_i)$. In line with recent reports on dual- and multi-resonant microwave biosensors, such feature-level fusion is expected to reduce the prediction error and enhance robustness, even when the per-band sensitivity is not maximized at each individual resonance.

Table 4 indicates that the proposed design offers a compact tri-band sensing mechanism with three distinct resonance features within the 2–6 GHz region, enabling multivariate calibration over an extended simulated glucose span (0–600 mg/dL). Compared with many reported microwave sensors that rely on a single or dual resonances [7–9, 15], the proposed approach provides additional independent information through the triplets (fr_1, fr_2, fr_3), which improves robustness to variations in thumb placement, contact pressure, and heterogeneous tissue loading. Moreover, the adopted multilayer thumb phantom model supports a more realistic on-body emulation than simple liquid-drop testing, facilitating the consistent assessment of glucose-dependent perturbations in a stratified biological environment [17, 20]. Overall, the combination of tri-band operation, quasi-linear frequency shifts, and a physiologically motivated thumb-loading configuration constitutes the main advantage of this study, offering improved feature redundancy and calibration stability relative to single-feature microwave sensing approaches.

4. CONCLUSION

This paper introduces a new thumb-coupled triple-band elliptical microstrip resonator for noninvasive microwave glucose sensing in the 2–6 GHz range. The coupling of the resonator has been realized by a capacitive technique. HFSS software is used to simulate the sensor and thumb model. The sensor demonstrates three glucose-sensitive resonances with monotonic and near-linear frequency responses over a wide range of 0–600 mg/dL. The frequency deviation rates were 0.147, 0.64, and 1.037 MHz/(mg/dL) for bands 1–3, respectively. The highest linearity was achieved in band 3 with $R^2 \approx 0.98$. The triple-band approach enables frequency-diverse sensing, allowing improved robustness through multivariate regression, which enhances the accuracy of measurements by utilizing data from all three bands simultaneously. Future work will focus on experimental validation and real-time on-body measurements.

REFERENCES

[1] World Health Organization, "Diabetes," Fact sheet, Nov. 2024.

[2] International Diabetes Federation, "IDF diabetes atlas," Brussels, Belgium, 2025.

[3] American Diabetes Association Professional Practice Committee for Diabetes, "7. Diabetes technology: Standards of care in diabetes — 2026," *Diabetes Care*, Vol. 49, No. Supplement_1, S150–S165, 2025.

[4] Natale, P., S. Chen, C. K. Chow, N. W. Cheung, D. Martinez-Martin, C. Caillaud, N. Scholes-Robertson, A. Kelly, J. C. Craig, G. Strippoli, and A. Jaure, "Patient experiences of continuous glucose monitoring and sensor-augmented insulin pump therapy for diabetes: A systematic review of qualitative studies," *Journal of Diabetes*, Vol. 15, No. 12, 1048–1069, 2023.

[5] Alahnomi, R. A., Z. Zakaria, Z. M. Yussof, A. A. Althuwayb, A. Alhegazi, H. Alsariera, and N. A. Rahman, "Review of recent microwave planar resonator-based sensors: Techniques of complex permittivity extraction, applications, open challenges and future research directions," *Sensors*, Vol. 21, No. 7, 2267, 2021.

[6] Liu, C., C. Liao, Y. Peng, W. Zhang, B. Wu, and P. Yang, "Microwave sensors and their applications in permittivity measurement," *Sensors*, Vol. 24, No. 23, 7696, 2024.

[7] Kiani, S., P. Rezaei, and M. Fakhr, "Dual-frequency microwave resonant sensor to detect noninvasive glucose-level changes through the fingertip," *IEEE Transactions on Instrumentation and Measurement*, Vol. 70, 1–8, 2021.

[8] Mohammadi, P., A. Mohammadi, and A. Kara, "Dual-frequency microwave resonator for noninvasive detection of aqueous glucose," *IEEE Sensors Journal*, Vol. 23, No. 18, 21 246–21 253, 2023.

[9] Farouk, M., A. S. A. El-Hameed, A. R. Eldamak, and D. N. Elsheakh, "Noninvasive blood glucose monitoring using a dual band microwave sensor with machine learning," *Scientific Reports*, Vol. 15, No. 1, 16271, 2025.

[10] Ong, W. M., S. S. Chua, and C. J. Ng, "Barriers and facilitators to self-monitoring of blood glucose in people with type 2 diabetes using insulin: A qualitative study," *Patient Preference and Adherence*, Vol. 8, 237–246, 2014.

[11] Janapala, R. N., J. S. Jayaraj, N. Fathima, T. Kashif, N. Usman, A. Dasari, N. Jahan, and I. Sachmechi, "Continuous glucose monitoring versus self-monitoring of blood glucose in type 2 diabetes mellitus: A systematic review with meta-analysis," *Cureus*, Vol. 11, No. 9, e5634, 2019.

[12] Shi, J., R. Fernández-García, and I. Gil, "Sensor technologies for non-invasive blood glucose monitoring," *Sensors*, Vol. 25, No. 12, 3591, 2025.

[13] Alsultani, A. B., K. Kovács, J. G. Chase, and B. Benyo, "Advances in invasive and non-invasive glucose monitoring: A review of microwave-based sensors," *Sensors and Actuators Reports*, Vol. 9, 100332, 2025.

[14] Singh, T., P. K. Mishra, A. Pal, and V. S. Tripathi, "A planar microwave sensor for noninvasive detection of glucose concentration using regression analysis," *International Journal of Microwave and Wireless Technologies*, Vol. 15, No. 8, 1343–1353, 2023.

[15] Kandwal, A., Z. Ju, L. W. Y. Liu, R. Jasrotia, C. K. Chan, Z. Nie, A. M. Almuhlafi, and H. Vettikalladi, "A dual-band microwave sensor for glucose measurements utilizing an enclosed split ring metamaterial-based array," *Engineering Science and Technology, an International Journal*, Vol. 62, 101947, 2025.

[16] Mansour, E., M. I. Ahmed, A. Allam, R. K. Pokharel, and A. B. Abdel-Rahman, "Sensitivity evaluation of a dual-finger metamaterial biosensor for non-invasive glycemia tracking on multiple substrates," *Sensors*, Vol. 25, No. 22, 7034, 2025.

[17] Krishnan, R., V. Selvaraj, N. Pandian, S. Sammandhan, I. U. Khan, and S. K. Oruganti, "A compact dielectric resonator antenna based microwave sensor for non-invasive blood glucose monitoring," *Instrumentation, Mesure, Metrologie*, Vol. 24, No. 5, 297–304, 2025.

[18] Soltanian, F., M. Nosrati, S. Mobayen, C.-C. Li, T. Pan, M.-T. Ke, and P. Skruch, "On-body non-invasive glucose monitoring sensor based on high figure of merit (FoM) surface plasmonic microwave resonator," *Scientific Reports*, Vol. 13, No. 1, 17527, 2023.

[19] Krishna, R. R., "A 3.1 GHz defected ground transmission line microwave sensor for blood glucose estimation," *Progress In Electromagnetics Research Letters*, Vol. 123, 83–88, 2025.

[20] Zaarour, Y., F. E. Arroud, T. Fernandez, J. L. Cano, R. E. Alami, O. E. Mrabet, A. Benani, A. Faik, and H. Griguer, "Microwave antenna sensing for glucose monitoring in a vein model mimicking human physiology," *Biosensors*, Vol. 15, No. 5, 282, 2025.